Modeling of molecular diffusion and thermal conduction with multi-particle interaction in compressible turbulence

Y. Tai, T. Watanabe, and K. Nagata

Citation: Physics of Fluids **30**, 035108 (2018); doi: 10.1063/1.5018248
View online: https://doi.org/10.1063/1.5018248
View Table of Contents: http://aip.scitation.org/toc/phf/30/3
Published by the American Institute of Physics

Modeling of molecular diffusion and thermal conduction with multi-particle interaction in compressible turbulence

Y. Tai, T. Watanabe,[a] and K. Nagata
Department of Aerospace Engineering, Nagoya University, Nagoya, Japan

(Received 5 December 2017; accepted 25 February 2018; published online 28 March 2018)

A mixing volume model (MVM) originally proposed for molecular diffusion in incompressible flows is extended as a model for molecular diffusion and thermal conduction in compressible turbulence. The model, established for implementation in Lagrangian simulations, is based on the interactions among spatially distributed notional particles within a finite volume. The MVM is tested with the direct numerical simulation of compressible planar jets with the jet Mach number ranging from 0.6 to 2.6. The MVM well predicts molecular diffusion and thermal conduction for a wide range of the size of mixing volume and the number of mixing particles. In the transitional region of the jet, where the scalar field exhibits a sharp jump at the edge of the shear layer, a smaller mixing volume is required for an accurate prediction of mean effects of molecular diffusion. The mixing time scale in the model is defined as the time scale of diffusive effects at a length scale of the mixing volume. The mixing time scale is well correlated for passive scalar and temperature. Probability density functions of the mixing time scale are similar for molecular diffusion and thermal conduction when the mixing volume is larger than a dissipative scale because the mixing time scale at small scales is easily affected by different distributions of intermittent small-scale structures between passive scalar and temperature. The MVM with an assumption of equal mixing time scales for molecular diffusion and thermal conduction is useful in the modeling of the thermal conduction when the modeling of the dissipation rate of temperature fluctuations is difficult. *Published by AIP Publishing.* https://doi.org/10.1063/1.5018248

I. INTRODUCTION

Mixing in compressible turbulence is an important phenomenon in various engineering applications as well as fundamental physics. It is well known that turbulence has a strong influence on mixing of diffusive scalars, such as mass fraction of chemicals and temperature[1] (e.g., mixing in jet engine). Understanding turbulent mixing and molecular diffusion in compressible turbulence is of great importance in practical problems such as a prior evaluation of interior air pollution of vehicles[2] and prediction of engine fuel efficiency.[3] The mixing process consists of turbulent diffusion stirring a fluid and molecular diffusion causing mixing at a molecular level. The rate of molecular diffusion is often controlled by turbulence since the generation of small scale structures by turbulence promotes the molecular diffusion. Compressibility has a strong influence on the molecular diffusion process in turbulence: turbulent activities such as vortical motions are attenuated by a fluid expansion due to heat release by chemical reactions;[4] the degree of intermittency in passive scalar fields increases as the turbulent Mach number increases.[5]

Development in computer technology enables us to use direct numerical simulations (DNSs) as one of the primary tools for studying turbulent mixing, especially for very small-scale features of turbulence, which is not easy to resolve in experiments. For practical problems, large eddy simulations (LESs) have advantages of a lower computational cost than DNS. The LES is also more suited for unsteady fluid phenomena than the approach based on Reynolds Averaged Navier-Stokes equations (RANS).[6] Therefore, the LES has been an essential tool in the computational fluid dynamics in many scientific and engineering fields. In the LES of turbulent reactive flows, a scalar field is divided into a resolved scale (grid scale, GS) and unresolved scale (subgrid scale, SGS), and the effects of unresolved scalar fluctuations must be taken into account to close the governing equation that includes filtered chemical source terms. Therefore, a closure, so-called SGS model, has attracted much attention for many years, and several proposals for closure methods for chemical source terms can be seen in previous studies.[7,8] However, it is not clear how these SGS models depend on the problem (e.g., different reaction schemes and different flow types). Recent progress in the LES of reactive flows relies on the methods implemented with an exact treatment of chemical source terms.[9] These simulations are often performed with Lagrangian notional particles to which scalar values are assigned.[10,11] The Lagrangian approaches require modeling molecular diffusion, whose model, called the mixing model, is also developed in the context of Lagrangian simulations combined with the LES.[12,13] There are various requirements which should be met by ideal mixing models. One of the foremost prerequisites is that they should be able to express a physical phenomenon of molecular diffusion with a simple calculation process. The mixing models should hold the essential nature of molecular diffusion, including conservation of mean scalar quantities, accurate scalar dissipation rates, and allowable values of scalar quantities determined by initial and boundary conditions.[9] Other examples of desirable features for mixing

[a]watanabe.tomoaki@c.nagoya-u.jp

models are providing Gaussian probability density function (PDF) of conserved scalar, continuous trajectories in a scalar composition space, and appropriate dependence on Reynolds and Schmidt numbers[9,14,15]

So far, most mixing models used in Lagrangian simulations rely on the process of interactions among Lagrangian particles. One of the examples is Curl's model based on two-particle interactions.[16] The Interaction by Exchange with the Mean (IEM) model, based on the relaxation of particle compositions toward the mean value, is also a simple and common model.[17] There are modified versions of these simple models, which overcome some shortcomings inhibited in the original models.[18,19] Recent progress in the development of mixing models has been achieved in terms of the localness in composition space, such as the Euclidean minimum spanning tree model,[20] shadow-position mixing model,[21] and multiple mapping conditioning model.[22] The locality in the composition space is important when the model is used in high-Damköhler-number cases such as combustion problems, where the molecular diffusion often controls the reaction rate. These models often minimize numerical diffusion caused by non-locality of modeled mixing events by introducing reference variables used in the selection of mixing particles. This is a more efficient way to ensure the locality of the mixing events than increasing the number of Lagrangian particles and enables us to simulate turbulent reactive flows with a small number of particles in sparse-Lagrangian particle methods at a moderate computational cost.

Almost all mixing models control the rate of mixing by a model parameter called mixing time scale τ_ϕ. Without an appropriate choice of τ_ϕ, mixing models fail to provide an accurate scalar dissipation rate, which is one of the requirements for the mixing models mentioned earlier. One of the common approaches for modeling τ_ϕ is based on the scalar-to-mechanical time scale ratio C_ϕ. However, previous studies have shown that C_ϕ is not a universal constant and C_ϕ used in existing literature exhibits a large variation depending on the problem.[23–25] In the implementation of the mixing model with the LES, C_ϕ needs to be locally defined as a function of space and time. Because of differences between velocity and scalar fields, which are described by different governing equations and different initial/boundary conditions, it is not surprising to observe a large spatiotemporal variation of C_ϕ in turbulent flows. Therefore, much attention should be paid to the method to determine τ_ϕ for further development of Lagrangian simulations of reactive flows with mixing models. In order to address this issue, the authors have proposed a mixing volume model (MVM)[26] based on the interaction between spatially distributed particles within a local and finite volume (mixing volume). The MVM uses the interaction by exchange with the local volume average, which is extended from the classical IEM model. The MVM enables us to calculate τ_ϕ that is dependent on space, time, and length scale of the mixing event. The extension of the MVM to Curl's type mixing scheme was also reported.[26,27] In the MVM, the mixing time scale is obtained from a reference scalar field simulated by a grid-based solver of the Navier-Stokes equations and convection-diffusion equation. The MVM has been utilized in conjunction with Lagrangian particle simulations (LPSs) and LES based on the approximate deconvolution model[28] or implicit LES.[26,27,29] It has been shown that the MVM provides a very accurate scalar dissipation rate under various conditions. These studies have confirmed that LES-LPS with the MVM based on two-particle interactions well reproduces the statistics of reactive scalars in planar jets[26] and scalar mixing layers[27] with a one-step isothermal irreversible reaction at both low and high Schmidt numbers. It has also been proved that the MVM with the multi-particle mixing scheme has a better performance than the two-particle mixing scheme on predicting molecular diffusion terms.[29] The LES-LPS with the MVM is expected to be a useful approach for predicting turbulent reactive flows at moderate computational costs because the MVM works well even at sparse conditions.

It should be noted that the MVM was developed for incompressible flows with constant density and constant diffusivity coefficient.[26,27,29] In this study, we consider the extension of the MVM to compressible turbulence, where density, viscosity, and diffusivity coefficient are no longer constants. We also consider the application of the MVM for modeling thermal conduction. We perform the DNS of compressible planar jets with a passive and inert scalar transfer for investigating the mixing process and the performance of the MVM. We present fundamental characteristics of molecular and thermal diffusions along with the results of *a priori* test of the MVM for molecular diffusion and thermal conduction. We will show that the MVM is very useful to model molecular and thermal diffusions on the Lagrangian notional particles in compressible flows. The paper is organized as follows. Section II describes the MVM extended for compressible flows. Section III presents the detail of the DNS of compressible planar jets. Section IV discusses the fundamental properties of compressible planar jets followed by the results of *a priori* test of the MVM in Sec. V B. The conclusions are summarized in Sec. VI.

II. MVM IMPLEMENTATION AND DIFFERENCE BETWEEN COMPRESSIBLE AND INCOMPRESSIBLE FLOWS

A. Governing equation for turbulent mixing in compressible turbulence

We briefly introduce the MVM for a compressible flow. The detail of the model formulated for incompressible flows can be found in our previous paper.[26] Here, we consider a passive scalar mixing problem described by Navier-Stokes equations for a compressible fluid and a conservation equation for passive scalar with an assumption of ideal gas, as shown in the following non-dimensional form:

$$\frac{\partial \rho}{\partial t} + \frac{\partial \rho u_j}{\partial x_j} = 0, \tag{1}$$

$$\frac{\partial \rho u_i}{\partial t} + \frac{\partial \rho u_i u_j}{\partial x_j} = -\frac{\partial P}{\partial x_i} + \frac{1}{Re}\frac{\partial \tau_{ij}}{\partial x_j}, \tag{2}$$

$$\frac{\partial \rho T}{\partial t} + \frac{\partial \rho T u_j}{\partial x_j} = -(\gamma - 1)P\frac{\partial u_j}{\partial x_j} + \frac{\gamma}{RePr}\frac{\partial}{\partial x_j}\left(k\frac{\partial T}{\partial x_j}\right) + \frac{\gamma - 1}{Re}\tau_{ij}\frac{\partial u_i}{\partial x_j}, \tag{3}$$

$$\frac{\partial \rho\phi}{\partial t} + \frac{\partial \rho\phi u_j}{\partial x_j} = \frac{1}{ScRe}\frac{\partial}{\partial x_j}\left(\rho D \frac{\partial \phi}{\partial x_j}\right), \tag{4}$$

$$P = \rho T. \tag{5}$$

Here, t is the time, x_i is the position, ρ is the density, u_i is the velocity, P is the pressure, T is the temperature, μ is the viscosity, k is the thermal conductivity, ϕ is the passive scalar, and D is the molecular diffusivity for ϕ, where non-dimensional variables are related to the dimensional counterparts as[30]

$$x_i = \frac{\tilde{x}_i}{l_r}, u_i = \frac{\tilde{u}_i}{u_r}, \rho = \frac{\tilde{\rho}}{\rho_r}, t = \frac{\tilde{t}u_r}{l_r}, P = \frac{\tilde{P}}{\rho_r u_r^2}, \tag{6}$$

$$T = \frac{\tilde{T}R}{u_r^2}, \phi = \frac{\tilde{\phi}}{\phi_r}, \mu = \frac{\tilde{\mu}}{\mu_r}, k = \frac{\tilde{k}}{k_r}, D = \frac{\tilde{D}}{D_r}, \tag{7}$$

where the subscript r refers to the reference quantity and $\gamma = c_p/c_v$ and $R = c_p - c_v$ are the ratio of the specific heat and the gas constant, respectively. The nondimensional parameters in the governing equations are the Reynolds number Re, Prandtl number Pr, and Schmidt number Sc defined by

$$Re = \frac{\rho_r u_r l_r}{\mu_r}, Pr = \frac{\mu_r c_p}{k_r}, Sc = \frac{\mu_r}{\rho_r D_r}. \tag{8}$$

For a Newtonian fluid, the viscous stress tensor τ_{ij} is represented by

$$\tau_{ij} = \mu\left(\frac{\partial u_i}{\partial x_j} + \frac{\partial u_j}{\partial x_i} - \frac{2}{3}\delta_{ij}\frac{\partial u_k}{\partial x_k}\right), \tag{9}$$

where δ_{ij} is the Kronecker delta.

B. MVM for molecular diffusion and thermal conduction

The MVM is developed for Lagrangian simulations of turbulent mixing, where N_P notional particles are used for simulating evolutions of passive scalar ϕ and temperature T. The state of the nth particle ($n = 1, \ldots, N_P$) is represented by position $\boldsymbol{x}^{(n)}$, passive scalar $\phi^{(n)} = \phi(\boldsymbol{x}^{(n)}(t); t)$, and temperature $T^{(n)} = T(\boldsymbol{x}^{(n)}(t); t)$ at the particle location, where the superscript (n) is used for identifying the particle. Under the governing equations (1)–(5), the particle evolves according to the following equation:

$$\frac{d\boldsymbol{x}^{(n)}}{dt} = \boldsymbol{u}^{(n)} = \boldsymbol{u}(\boldsymbol{x}^{(n)}(t); t), \tag{10}$$

$$\frac{d\phi^{(n)}}{dt} = \left[\frac{1}{ReSc}\frac{1}{\rho}\nabla\cdot(\rho D\nabla\phi)\right]^{(n)} = [D_\phi]^{(n)}, \tag{11}$$

$$\frac{dT^{(n)}}{dt} = \left[\frac{\gamma}{RePr}\frac{1}{\rho}\nabla\cdot(k\nabla T)\right]^{(n)} + \left[S_{hspd}\right]^{(n)} = [D_T]^{(n)} + \left[S_{hspd}\right]^{(n)}, \tag{12}$$

where D_ϕ, D_T, and S_{hspd} are the molecular diffusion term, thermal conduction term, and high-speed source term for temperature.[31] When the velocity field $\boldsymbol{u}(\boldsymbol{x}, t)$ is given from other simulations or models, Eq. (10) can be integrated with time. However, $[D_\phi]^{(n)}$, $[D_T]^{(n)}$, and $[S_{hspd}]^{(n)}$ cannot be represented by the quantities at the particle location because of spatial derivatives. Therefore, the MVM for compressible flows is developed for modeling $[D_\phi]^{(n)}$ and $[D_T]^{(n)}$ below. S_{hspd} represents the effects of the heating or cooling of a fluid via compression or expansion and viscous heating. Further details of the modeling of S_{hspd} can be found in other papers.[31]

The molecular diffusion effect for a particle n is modeled by the interaction with mixing particles within a finite volume (mixing volume) V_m^n (Fig. 1). We consider a volume average of variable f within the mixing volume V_m^n, denoted by $\langle f|V_m^n\rangle$, which is calculated from notional particles with a kernel function $G_n(\boldsymbol{x}^{(m)})$ as

$$\langle f|V_m^n\rangle = \frac{\sum_{m=1}^{N_P} G_n(\boldsymbol{x}^{(m)}) f^{(m)}}{\sum_{m=1}^{N_P} G_n(\boldsymbol{x}^{(m)})}, \tag{13}$$

$$G_n(\boldsymbol{x}^{(m)}) = \begin{cases} 1, \text{ if } \boldsymbol{x}^{(m)} \text{ is in mixing volume } V_m^n \\ 0, \text{ otherwise} \end{cases}. \tag{14}$$

In the MVM, the effect of molecular diffusion on $\phi^{(n)}$ is modeled by a relaxation process toward the average in the mixing volume, $\langle\phi|V_m^n\rangle$, as

$$\left[D_\phi\right]_{\text{mix}}^{(n)} = \frac{1}{\tau_\phi}\left(\langle\phi|V_m^n\rangle - \phi^{(n)}\right), \tag{15}$$

$$\tau_\phi = \frac{\langle\phi''^2|V_m^n\rangle}{\langle\varepsilon_\phi|V_m^n\rangle}, \tag{16}$$

where the subscript "mix" represents the quantity modeled by the mixing model, $f'' = f^{(n)} - \langle f|V_m^n\rangle$ denotes a fluctuation from the mean value within the mixing volume, and $\tilde{\varepsilon}_\phi = \tilde{D}\nabla\tilde{\phi}\cdot\nabla\tilde{\phi}$ is the passive scalar dissipation rate. The mixing time scale τ_ϕ controls the rate of molecular diffusion. The expression of τ_ϕ in Eq. (16) is obtained from the transport equation for $\langle\phi''^2|V_m^n\rangle$, and thus $\langle\phi''^2|V_m^n\rangle$ decays at the rate given by the mean scalar dissipation rate within the mixing volume.[29] One of the important differences from incompressible cases arises from density and temperature variations, which result in a variable diffusivity coefficient D. This requires the model to use fluid properties at each particle location $\mu^{(n)}$, $\rho^{(n)}$, and $T^{(n)}$.

The mixing volume model can be applied for the thermal conduction term by analogy with the molecular diffusion term as

$$[D_T]_{\text{mix}}^{(n)} = \frac{1}{\tau_T}\left(\langle T|V_m^n\rangle - T^{(n)}\right), \tag{17}$$

$$\tau_T = \frac{\langle T''^2|V_m^n\rangle}{\langle\varepsilon_T|V_m^n\rangle}, \tag{18}$$

where $\tilde{\varepsilon}_T = (\tilde{k}/\tilde{\rho})\nabla\tilde{T}\cdot\nabla\tilde{T}$ is the dissipation rate of temperature fluctuation per unit mass, where k is also locally evaluated at the particle location as $k^{(n)}$.

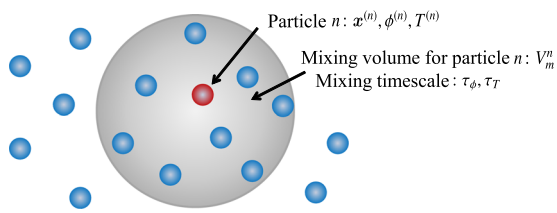

FIG. 1. Schematic of the mixing volume model in compressible flows.

The volume average used in the MVM is simply related to the ensemble average of particles that participate in the mixing event, and an arbitrary shape of the mixing volume can be used in the model. The following procedure[29] is useful in the application of the MVM: (1) decide the number of the mixing particles, N_m, in one mixing event with particle n; (2) choose $N_m - 1$ mixing particles in the descending order according to the distance from the particle n; and (3) compute the MVM based on the ensemble average of the selected particles. In this procedure, the choice of the mixing particles determines the model performance, where selecting the mixing particles can be done by using a sorting algorithm. It should be noted that conventional mixing models often use the sorting algorithm for selecting the mixing particles.[10,12] Then, the computational time of the MVM depends on a particular algorithm used for sorting and is expected to be almost the same order of magnitude as conventional models.

III. DNS OF TEMPORALLY EVOLVING COMPRESSIBLE PLANAR JETS

A. Temporally evolving compressible planar jets

We perform the DNS of temporally evolving compressible planar jets with a passive scalar transfer. The DNS is utilized to produce database of compressible turbulence, which is used in *a priori* test of the MVM and investigation of compressibility effects on diffusive processes.

The present DNS is carried out with a three-dimensional rectangular computational domain. The streamwise, lateral, and spanwise directions are represented by x, y, and z, respectively. The size of the computational domain is $(L_x \times L_y \times L_z)$. The origin of the Cartesian coordinate system is located at the center of the y-z plane on the one side of the boundary of the computational box, where the streamwise coordinate is $0 \le x \le L_x$. The flow is periodic in the streamwise and spanwise directions.

The initial mean velocity profile is described by

$$\langle \tilde{u} \rangle = 0.5U_J + 0.5U_J \tanh\left(\frac{H - 2|\tilde{y}|}{4\theta_J}\right), \tag{19}$$

where U_J is the initial jet velocity, H is the initial jet width (slit width), and $\theta_J = 0.03H$ is the initial shear layer thickness between the jet and the ambient fluid. $\langle\cdot\rangle$ denotes the averaged value taken in the homogeneous directions. The initial velocity field is generated by superimposing the velocity fluctuations on the mean velocity profile, where the inflow generator based on a diffusion process[32] is implemented to generate the fluctuating components in the region of $|y| \le 0.5H$. The characteristic length scale of the velocity fluctuation is $0.5H$, and the root-mean-squared (rms) velocity fluctuation is $0.02U_J$. Similarly, the following profile is used for the passive scalar profile:

$$\tilde{\phi} = 0.5\phi_J + 0.5\phi_J \tanh\left(\frac{H - 2|\tilde{y}|}{4\theta_J}\right), \tag{20}$$

where ϕ_J is the scalar value in the planar jet. The pressure at the initial state is uniform and equal to the standard atmospheric pressure $P_a = 1.013 \times 10^5$ (Pa). The temperature in the ambient fluid T_a and near the jet centerline T_J is 300 K, while the temperature profile in the shear layers follows the Crocco-Busemann relation. The following fluid properties are used in the present DNS: the gas constant $R = 287$ [J/(kg · K)]; the ratio of specific heats $\gamma = 1.4$; the Prandtl number $Pr = 0.7$. Then, the initial density field is calculated from Eq. (5). We consider $Sc = 1$ for ϕ. The viscosity $\tilde{\mu}$ is given by Sutherland's law,

$$\frac{\tilde{\mu}}{\mu_0} = \left(\frac{\tilde{T}}{T_0}\right)^{3/2} \frac{T_0 + S}{\tilde{T} + S}. \tag{21}$$

$\mu_0 = 1.724 \times 10^{-5}$ (Pa · s) is the shear viscosity at $T_0 = 273$ (K) and Sutherland's constant is $S = 110.4$ (K). We can obtain the local speed of sound in the jet $c_J = \sqrt{\gamma R T_J}$ and in the ambient flow $c_a = \sqrt{\gamma R T_a}$. The reference quantities in Eq. (7) are chosen as

$$l_r = H, u_r = U_J, \rho_r = \frac{P_a}{RT_a}, \phi_r = \phi_J, \mu_r = \mu_0, k_r = \frac{\mu_0 c_p}{Pr}, D_r = \frac{\mu_0}{\rho_r Sc}. \tag{22}$$

The Reynolds number and the Mach number of planar jets are defined as $Re_J = \rho_J U_J H/\mu_J$ and $M_J = U_J/c_J$, respectively, where $\rho_J = P_a/RT_J$ and μ_J are the density and viscosity on the jet centerline.

B. Computational methods and conditions

The DNS is performed for four sets of parameters (Re_J, M_J) summarized in Table I, where the number of the grid points is denoted by $(N_x \times N_y \times N_z)$. The governing equations are numerically solved with the DNS code based on fully explicit methods proposed by Wang *et al.*[33,34] The present code is parallelized with the message passing interface (MPI), where the 2D pencil decomposition is applied with the x-pencil orientation.[35] The grid spacing is uniform in the x and z directions, whereas the grid location in the y direction is given from the integer $j = 1, \ldots, N_y$ using the following mapping function:

$$y(j) = -\frac{L_y}{2\alpha_y} \text{a tanh}\left\{(\tanh \alpha_y)\left[1 - 2\left(\frac{j-1}{N_y - 1}\right)\right]\right\}. \tag{23}$$

Here, we use $\alpha_y = 4$. The periodic boundary conditions are applied in the x and z directions. Pressure waves are radiated from compressible jets and reach the lateral boundaries. These waves can distort the jet flow region by reflecting at the boundaries unless non-reflecting boundary conditions are applied. In this study, the subsonic non-reflecting outflow boundary of the Navier-Stokes characteristic boundary condition[36] (NSCBC) is applied with a sponge layer, where the second-order low-pass filter[34] suppresses the fluctuations on the grid stretched in the y direction. The sponge layers with the width of $8H$ are set up for the boundaries in the y directions.

The present DNS code is based on the fully explicit numerical schemes used in the DNS by Wang *et al.*[33] The computation of spatial derivatives is based on an 8th-order explicit finite difference scheme.[37] The region near the boundaries is treated with an internal-biased lower-order scheme to maintain numerical stability except for the boundaries with the periodic conditions.[33] An explicit five-step fourth-order Runge-Kutta scheme[36] is used for marching time step of Euler terms

TABLE I. Physical and computational parameters of the DNS. The displayed turbulence characteristics are taken from the jet centerline at $t = 22H/U_J$ ($Re_J = 14\,000$) and $t = 18H/U_J$ ($Re_J = 32\,000$), where the turbulent Mach number $M_T = \langle u_i'' u_i'' \rangle^{1/2}/\langle c \rangle$ (speed of sound: $\tilde{c} = \gamma R \tilde{T}$) and the turbulent Reynolds number $Re_\lambda = \langle \tilde{\rho} \rangle \langle \tilde{u}''^2 \rangle^{1/2} \tilde{\lambda}/\langle \tilde{\mu} \rangle$ (Taylor microscale: $\lambda = \langle u'^2 \rangle^{1/2}/\langle (\partial u'/\partial x)^2 \rangle^{1/2}$).

	Run A	Run B	Run C	Run D
Re_J	14 000	14 000	14 000	32 000
M_J	0.6	1.6	2.6	1.6
Sc	1.0	1.0	1.0	1.0
Pr	0.7	0.7	0.7	0.7
L_x, L_y, L_z	$12H, 30H, 6H$	$12H, 30H, 6H$	$12H, 30H, 6H$	$6H, 26H, 4H$
N_x, N_y, N_z	2 200, 1 400, 1 100	2 200, 1 400, 1 100	2 200, 1 400, 1 100	2 100, 2 300, 1 400
Time step dt	$1.2 \times 10^{-3} H/U_J$	$2.3 \times 10^{-3} H/U_J$	$2.6 \times 10^{-3} H/U_J$	$1.1 \times 10^{-3} H/U_J$
$\Delta_x = \Delta_z$	1.46η	1.32η	1.17η	1.46η
η	$3.7 \times 10^{-3} H$	$4.1 \times 10^{-3} H$	$4.7 \times 10^{-3} H$	$2.0 \times 10^{-3} H$
Re_λ	117	112	109	228
Ma_T	0.11	0.28	0.45	0.36

including convection and pressure term, while the other terms arising from the viscous effects, molecular diffusion, and thermal conduction are handled with an explicit first-order Euler scheme. In order to minimize an aliasing error, which is related to an unphysical growth of the spectral energy content of the integration variables at high wave numbers, the convective terms are calculated with a cubic skew-symmetric formulation[38] and an explicit tenth-order filter[37] is applied at the end of each time step.

Table I also shows the statistical properties of turbulence in the self-similar regime of the jet (at $t = 22$ for $Re_J = 14\,000$ and 18 for $Re_J = 32\,000$). The computational grid size is small enough to capture the smallest scale of turbulence represented by the Kolmogorov length scale $\tilde{\eta} = (\langle \tilde{\mu} \rangle/\langle \tilde{\rho} \rangle)^{3/4} \langle \tilde{\varepsilon} \rangle^{-1/4}$, where $\tilde{\varepsilon} = \tilde{\tau}_{ij} \tilde{S}_{ij}/\tilde{\rho}$ is the kinetic energy dissipation rate per unit mass and $\tilde{S}_{ij}$ is the strain-rate tensor.

IV. DNS RESULTS OF COMPRESSIBLE PLANAR JETS

A. Temporal evolutions of compressible planar jets

Figure 2 visualizes passive scalar ϕ on an x-y plane. From the lateral distribution of ϕ, we can find that the diffusion of ϕ is slower for higher Mach number as confirmed by larger ϕ near the centerline for higher M_J cases. It is also clear that the smaller scale structures appear for the higher Re case because the smallest length scale for the scalar field decreases with the Reynolds number. Figure 3 visualizes temperature $\tilde{T}/T_J$ at $t = 22$ on an x-y plane. The temperature in the jet is increased from the initial value T_J. The temperature field in the jet also exhibits a wide range of scales. The structures of temperature fluctuation outside the jet strongly depend on M_J: shock-like structures can be found for higher M_J in Fig. 3(b). Temperature fields at $t = 22$ are used for testing the MVM for thermal conduction.

Figure 4 shows the temporal evolution of the jet half width defined with the mean streamwise velocity and mean scalar profiles, which are denoted by b_U and b_ϕ, respectively. In a self-similar regime of temporally evolving jets, b_U and b_ϕ change with the square root of t.[43] The present DNS also shows that ${b_U}^2$ and ${b_\phi}^2$ linearly change with time after the jet is developed. Hence, we compute the slope of the curve in Fig. 4(a) in the self-similar regime, as summarized in Table II in comparison with the temporal DNS of an incompressible planar jet.[43] Small variations of the slope can be found depending on the condition. Previous studies also show the dependence of the jet evolution on the inflow condition.[44] Statistics obtained in temporal simulations are often moderately converged because of a finite size of a computational domain.[45,46] This results in a small temporal variation of the slope in Fig. 4 in later time, for which the computational domain contains the smaller number of large-scale structures. The influence of Mach number observed in the visualization is also confirmed from the jet half width: At a given time, the jet width is narrower for higher Mach numbers. This is explained by the potential core region that lasts longer for higher Mach numbers because of delayed transition to the turbulent jet.

The statistics in a fully developed region ($t = 22$ for $Re_J = 14\,000$ and $t = 18$ for $Re_J = 32\,000$) are examined below. Figure 5 compares the self-similar profile of mean velocity $\langle u \rangle$ and mean scalar $\langle \phi \rangle$ with experiments of incompressible planar jets, where the variables along the abscissa and the ordinate are normalized by the half width and the mean value on the centerline, $\langle \cdot \rangle_C$, respectively. The well-known profiles of $\langle u \rangle$ and $\langle \phi \rangle$ are obtained in the present DNS. The rms values of velocity and scalar fluctuations, denoted by subscript rms, are also compared with previous studies of incompressible planar jets in Fig. 6.[40–42,47] Although overall profiles are similar in all cases of the DNS, the rms velocity fluctuations divided by the mean centerline velocity decrease with the Mach numbers. The Mach number influence is stronger for the lateral component v_{rms}. A decrease in turbulent velocity fluctuations due to compressibility was also found in compressible shear layers.[48]

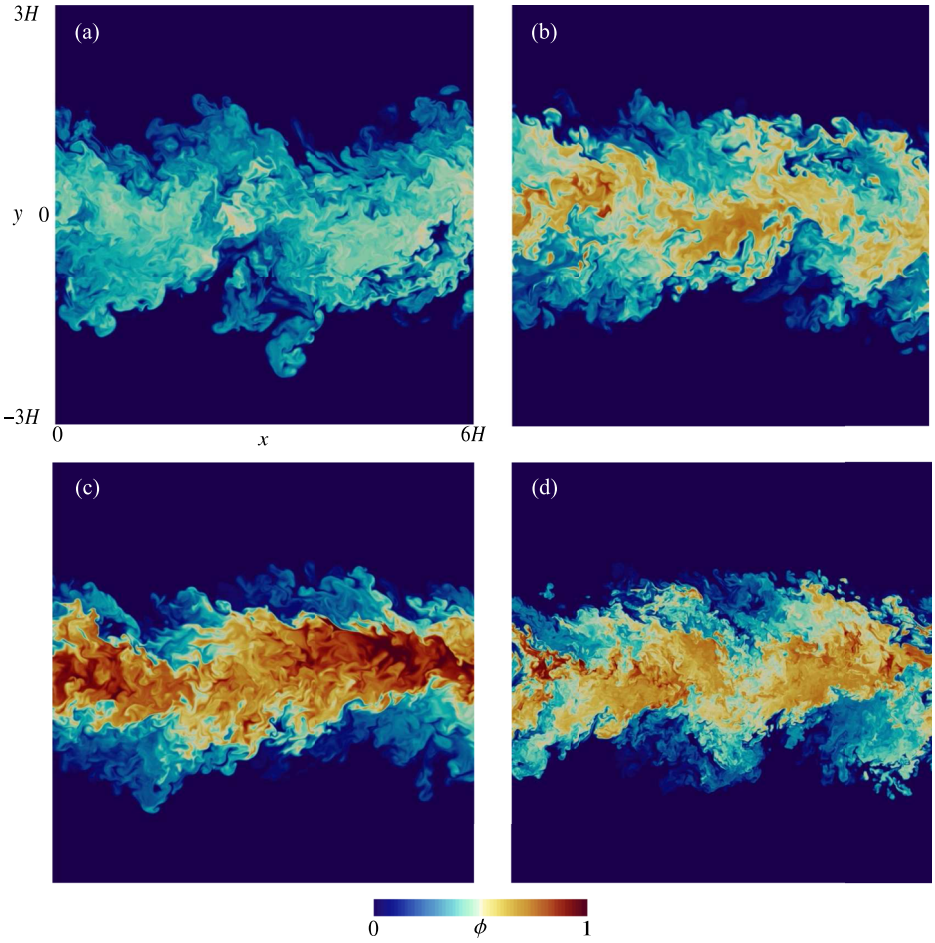

FIG. 2. Visualization of the passive scalar field for (a) Run A (t = 22), (b) Run B (t = 22), (c) Run C (t = 22), and (d) Run D (t = 18) at z = 0.

B. Small-scale properties of passive scalar and temperature

The MVM is applied to the thermal and molecular diffusions. The turbulence enhances the diffusion by producing small-scale structures, where the scalar gradient is amplified via the coupling of scalar and velocity fields. This can be examined with the production term of the dissipation rate of passive scalar fluctuation,

$$P_\phi = -\frac{\partial\phi}{\partial x_i}S_{ij}\frac{\partial\phi}{\partial x_j} = -\frac{\partial\phi}{\partial x_i}S^*_{ij}\frac{\partial\phi}{\partial x_j} - \frac{1}{3}\frac{\partial\phi}{\partial x_i}\frac{\partial\phi}{\partial x_i}S_{kk} \equiv P^*_\phi + P^d_\phi, \tag{24}$$

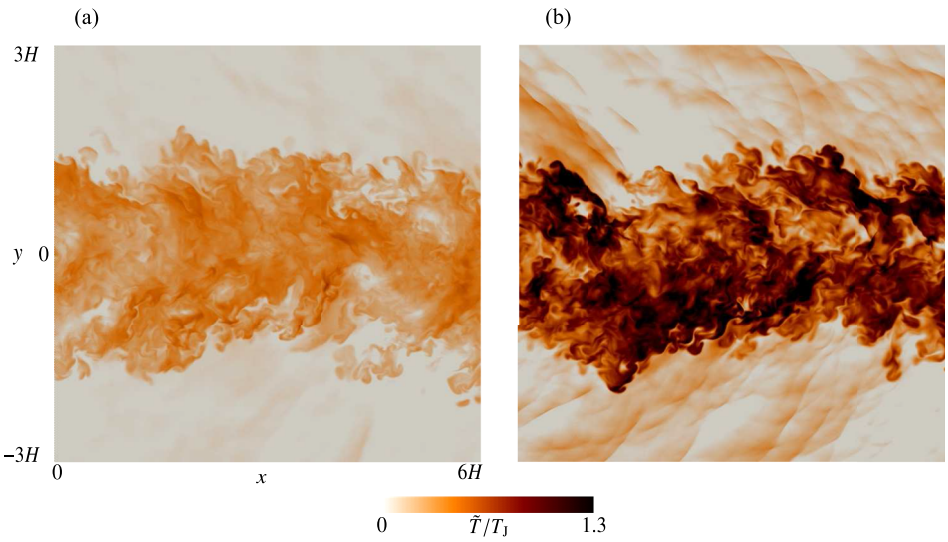

FIG. 3. Visualization of temperature field for (a) Run B (t = 22) and (b) Run C (t = 22) at z = 0.

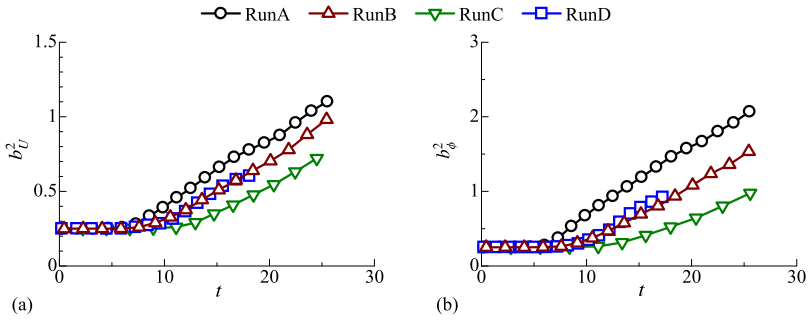

FIG. 4. Temporal evolutions of the jet half width defined with the lateral profile of (a) mean streamwise velocity (b_U) and (b) mean scalar (b_ϕ).

TABLE II. Slope of the curve in Fig. 4(a) in the self-similar regime, where $b_U{}^2$ linearly increases with time. The table also includes the result from the temporal DNS of the incompressible planar jet.[43]

	Run A	Run B	Run C	Run D	Reference 43
Slope	0.0416	0.0451	0.0386	0.0409	0.0569

where S_{ij}^* is the solenoidal components of the rate of strain tensor. The first term P_ϕ^* arises from a fluid deformation without direct effects of compressibility, while the second term P_ϕ^d is related to fluid expansion and compression from compressible effects. Similarly, the production term for the dissipation rate of temperature fluctuation can be written as

$$P_T = -\frac{\partial T}{\partial x_i} S_{ij} \frac{\partial T}{\partial x_j} = -\frac{\partial T}{\partial x_i} S_{ij}^* \frac{\partial T}{\partial x_j} - \frac{1}{3} \frac{\partial T}{\partial x_i} \frac{\partial T}{\partial x_i} S_{kk} = P_T^* + P_T^d. \tag{25}$$

Figure 7 shows the probability density functions (PDFs) of P_ϕ^*, P_ϕ^d, P_T^*, and P_T^d normalized with $\langle S_{ij}^* S_{ij}^* \rangle_c$ and $\langle \nabla\phi \cdot \nabla\phi \rangle_c$ or $\langle \nabla T \cdot \nabla T \rangle_c$. We can find positively skewed PDF of P_ϕ^* and P_T^*, which is also found in previous studies of incompressible turbulence.[49,50] As the Mach number increases, the contribution of P_ϕ^d and P_T^d to the total production terms becomes large. However, the production of the scalar dissipation rate denoted by positive P_ϕ and P_T is still dominated by the solenoidal parts P_ϕ^* and P_T^*. In all DNSs, the PDFs of P_ϕ^* and P_T^* collapse very well, and there is a statistical similarity between the productions of the dissipation rate of passive scalar and temperature fluctuations. This result strongly motivates us to use the MVM, originally developed for the molecular diffusion, to the thermal conduction, which is very active in the region with a large temperature gradient. A structural similarity of highly dissipative regions for passive scalar and temperature was also found in the previous study.[5]

V. *A PRIORI* TESTS OF MVM IN COMPRESSIBLE JETS

A. Evaluation methods of mixing volume model

The performance of the MVM is tested for molecular diffusion and thermal conduction in the fully developed regime of compressible planar jets. The detail of *a priori* test is described here. We consider a spherical mixing volume with a radius r_m (Fig. 8) whose center is located on the jet centerline. We consider N_m particles within the mixing volume. The location of the 1st particle $\boldsymbol{x}^{(1)}$ shown with red in Fig. 8 is the center of the sphere while the other particles (blue) are randomly distributed within the mixing volume ($|\boldsymbol{r}^{(n)}| = |\boldsymbol{x}^{(n)} - \boldsymbol{x}^{(1)}| \le r_m$). The variables at the particle locations are obtained with a tri-linear interpolation of DNS data. The molecular diffusion and thermal conduction terms approximated by the MVM are computed for particle 1 following Eqs. (15) and (17). These terms computed with the MVM are denoted with the subscript mix. These are compared with the molecular diffusion and thermal conduction terms directly computed with a finite difference approximation (8th-order central difference scheme), where the values obtained with a finite difference approximation is referred to as the DNS value.

The spheres placed on different locations are used for taking an ensemble average. For better statistical convergence, five sets of positions of N_m particles are considered for one mixing volume, where each set is used for computing the molecular and thermal conduction terms. The MVM is tested for a wide range of r_m and N_m with all DNSs in Table I, where the minimum values of r_m and N_m are 4η and 2, respectively.

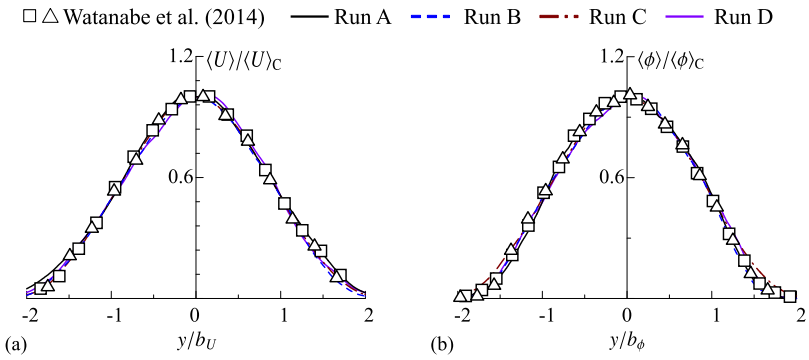

FIG. 5. Self-similar profiles of (a) mean streamwise velocity and (b) mean passive scalar, where subscript c denotes a value on the centerline. The present DNS is compared with experiments of incompressible planar jets.[39]

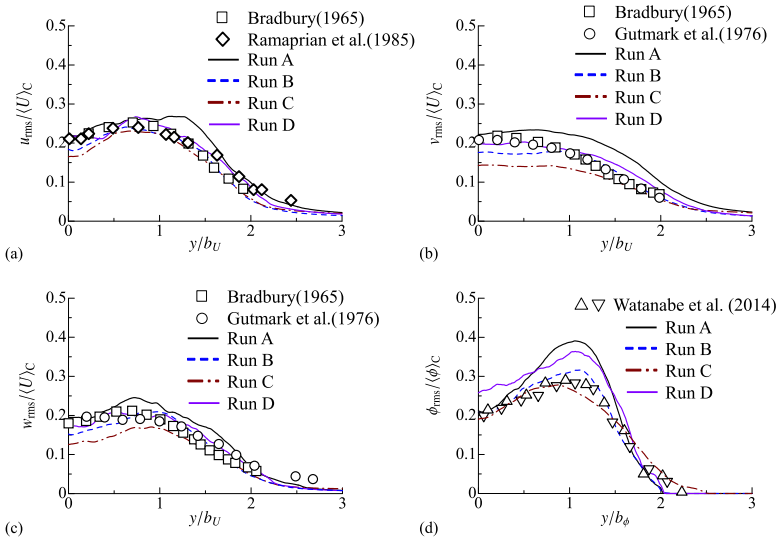

FIG. 6. Self-similar profiles of (a) rms streamwise velocity fluctuation, (b) rms lateral velocity fluctuation, (c) rms spanwise velocity fluctuation, and (d) rms passive scalar fluctuation. The present DNS is compared with experiments of planar jets.[39–42]

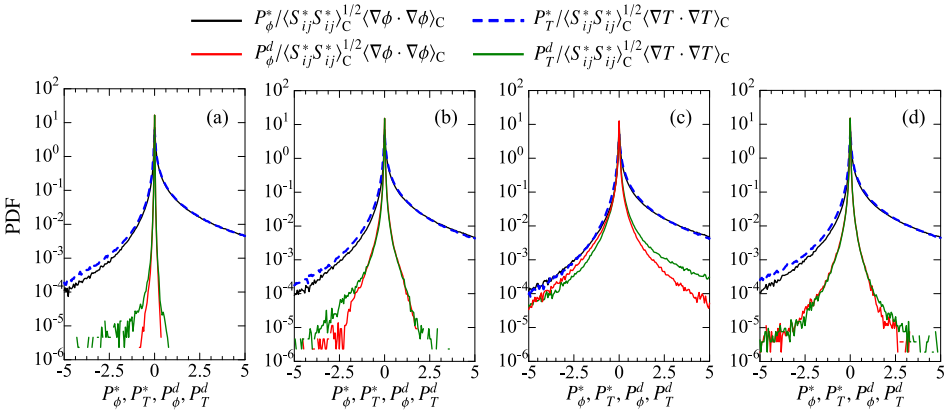

FIG. 7. PDF of P^*_ϕ, P^*_T, P^d_ϕ, and P^d_T, which are normalized by $\langle S^*_{ij}S^*_{ij}\rangle_c^{1/2}\langle\nabla\phi\cdot\nabla\phi\rangle_c$ or $\langle S^*_{ij}S^*_{ij}\rangle_c^{1/2}\langle\nabla T\cdot\nabla T\rangle_c$. The PDFs are computed on the centerline from (a) Run A, (b) Run B, (c) Run C, and (d) Run D.

B. Results and discussions

We use a correlation coefficient between the DNS and MVM values (D_a and $[D_a]_{\rm mix}$ with $a=\phi$ or T) defined as

$$\text{Correlation coefficient} = \frac{\left\langle D'_a [D_a]'_{\rm mix}\right\rangle}{\sqrt{\langle (D_a')^2\rangle\left\langle ([D_a]'_{\rm mix})^2\right\rangle}}, \qquad (26)$$

where $f' = f - \langle f\rangle$ denotes the fluctuation from the mean value. Figure 9 shows the correlation coefficient for D_ϕ as a function of (N_m, r_m). The magnitude of the correlation coefficient in Fig. 9 is almost the same as in incompressible planar jets, for which LES-LPS with the MVM well predicts temporal evolutions of mean scalar and scalar variance.[29] Therefore, we can expect that the MVM works well in the LPS of compressible flows. The correlation becomes higher with an increase in N_m and a decrease in r_m/η while the correlation is almost 0 for $N_m = 2$. The magnitude of the correlation coefficients in the present DNS is similar to the one obtained in incompressible jets.[29] Even in the compressible flow, the accuracy of MVM is improved as the particle density of the mixing volume increases. However, the sensitivity of the MVM performance to the Mach number is also clear especially when N_m becomes large ($N_m \geq 15$), where the correlation coefficient decreases with the Mach number. Figures 10 and 11 show the joint PDF of $[D_\phi]_{\rm mix}$ and D_ϕ obtained for $N_m = 2$ and 14, respectively. The shape of the joint PDF drastically changes from $N_m = 2$ to 14. A large probability is found for 1st and 3rd quadrants for $N_m = 14$ in Fig. 11, and thus a positive correlation between D_ϕ and $[D_\phi]_{\rm mix}$ is confirmed as in the correlation coefficients while a large probability is also found for 2nd and 4th quadrants for $N_m = 2$.

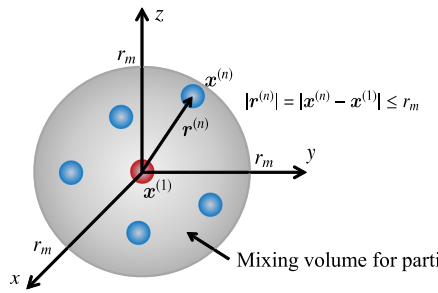

FIG. 8. *A priori* test of the mixing volume model with the DNS database.

Figures 12 and 13 show the PDF of mixing time scale τ_ϕ used in the MVM for $Re = 14\,000$. τ_ϕ hardly depends on the Mach number. In the case of $N_m = 2$, the PDF has a peak at $\tau_\phi = 0$, which leads to a discontinuous jump in the passive

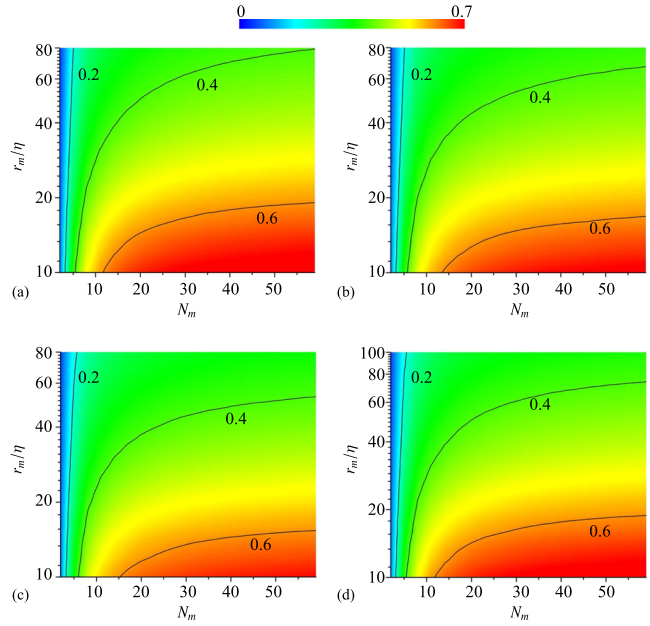

FIG. 9. Correlation coefficients between DNS and MVM values (D_ϕ and $[D_\phi]_{\rm mix}$) of molecular diffusion terms as a function of (N_m, r_m) on the jet centerline in (a) Run A (b) Run B, (c) Run C, and (d) Run D. Solid lines are isolines of correlation coefficients equal to 0.2, 0.4, and 0.6.

scalar composition space and causes unrealistic intense mixing events. This results in the weak correlation for $N_m = 2$ in Fig. 9. For $N_m = 8$ and 14, τ_ϕ tends to be larger than zero, and the mixing gradually occurs. Comparison between Figs. 12 and 13 shows that in the case of $N_m = 8$ or 14, a probability for $\tau_\phi \approx 1$ and $\tau_\phi \gg 1$ is, respectively, higher and lower for $r_m = 14\eta$ than that for 70η. Thus, a smaller mixing volume with more than two mixing particles results in fast mixing without a discontinuous jump in the composition space.

A mean contribution of molecular diffusion can be examined with the conditional average of D_ϕ on ϕ, denoted by $\langle D_\phi|\phi\rangle$. The conventional average $\langle D_\phi\rangle$ is related to $\langle D_\phi|\phi\rangle$ with the pdf of ϕ, $p(\phi)$, as $\langle D_\phi\rangle = \int_0^1 p(\phi)\langle D_\phi|\phi\rangle d\phi$. Figure 14 shows the molecular diffusion density in ϕ-space, $p(\phi)\langle D_\phi|\phi\rangle$, against the passive scalar fluctuation $\phi' = \phi - \langle\phi\rangle$. Under various conditions, the MVM well predicts the mean contribution of the molecular diffusion conditioned on the value of ϕ. It is also found that the agreement between the DNS and the MVM is slightly degraded for $\phi' > 0$ for $M_{\rm J} = 2.6$, and smaller mixing volumes are required for higher Mach number cases.

The compressible turbulence can be characterized by large density fluctuations due to fluid expansion/compression, which can be described by dilatation $\nabla\cdot\boldsymbol{u}$. We examine the performance of the MVM for regions with strong and weak fluid expansion or compression, which is distinguished by $\Theta = |\nabla\cdot\boldsymbol{u}|$. We consider the mixing volume with $r = 4\eta$, where the correlation coefficients are separately computed for the mixing volume with $\langle\Theta|V_m^n\rangle > 0.5$ (strong case) and $\langle\Theta|V_m^n\rangle < 0.1$ (weak case) from Run C as shown in Fig. 15. These thresholds are determined based on the average of Θ on the centerline. The figure also includes the correlation coefficient obtained from all mixing volumes. The correlation coefficients are very similar for both strong and weak cases, and direct influences of strong events of fluid expansion/compression are small for the MVM.

An *a priori* test is also performed at $y = b_\phi$, where both turbulent and non-turbulent fluids appear.[51,52] The intermittent region plays an important role in non-premixed flame because the isosurface of the stoichiometric mixture fraction often appears near the interface between turbulent and non-turbulent fluids.[53] Figure 16(a) shows the correlation coefficient between D_ϕ and $[D_\phi]_{\rm mix}$ at $y = b_\phi$ at $t = 22$ (Run B). The correlation coefficient is very similar at $y = 0$ (Fig. 9) and $y = b_\phi$ (Fig. 16). Similar to Fig. 14, the molecular diffusion

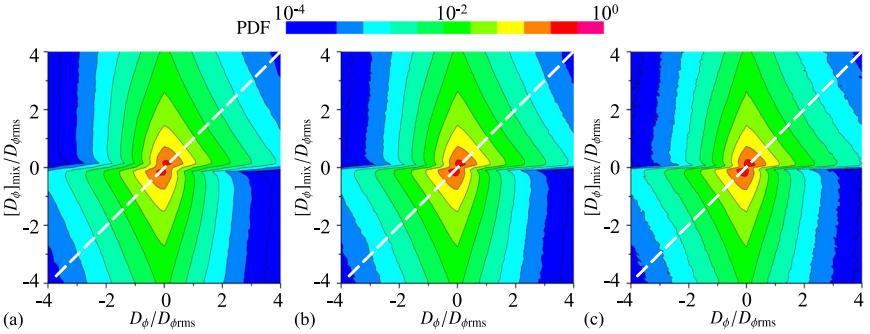

FIG. 10. Joint probability density functions of DNS and MVM values (D_ϕ and $[D_\phi]_{\rm mix}$) of molecular diffusion terms for $N_m = 2$ and $r_m = 14\eta$ on the jet centerline in (a) Run A (b) Run B, and (c) Run C. The broken line denotes $D_\phi = [D_\phi]_{\rm mix}$. The molecular diffusion term is normalized by the rms value of its fluctuation denoted by $D_{\phi\,\rm rms}$.

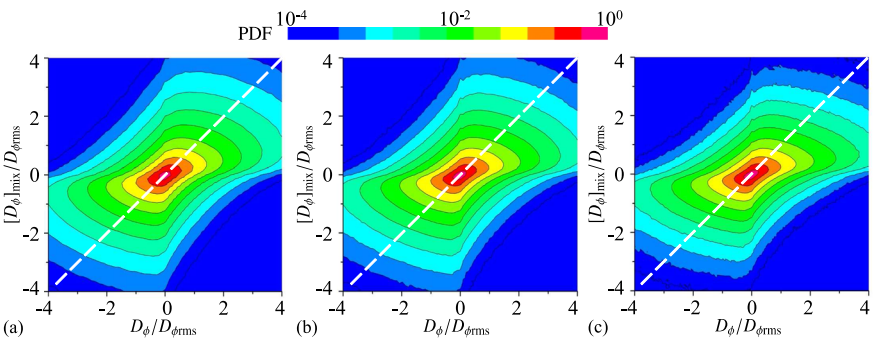

FIG. 11. The same plots as in Fig. 10 but for the MVM with $N_m = 14$ and $r_m = 14\eta$ on the jet centerline in (a) Run A (b) Run B, and (c) Run C.

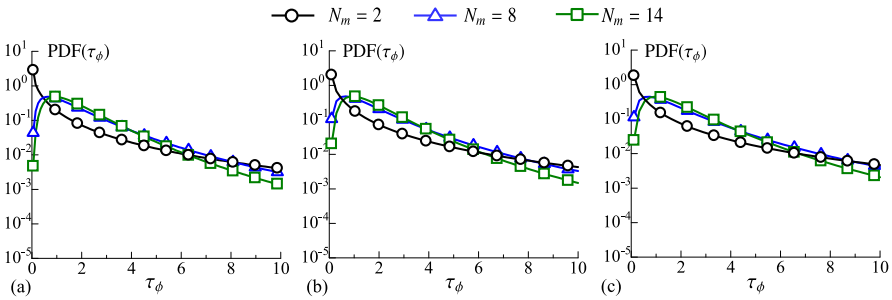

FIG. 12. Probability density functions of the mixing time scale τ_ϕ for $r_m = 14\eta$ on the jet centerline in (a) Run A, (b) Run B, and (c) Run C. The results are shown for N_m = 2, 8, and 14.

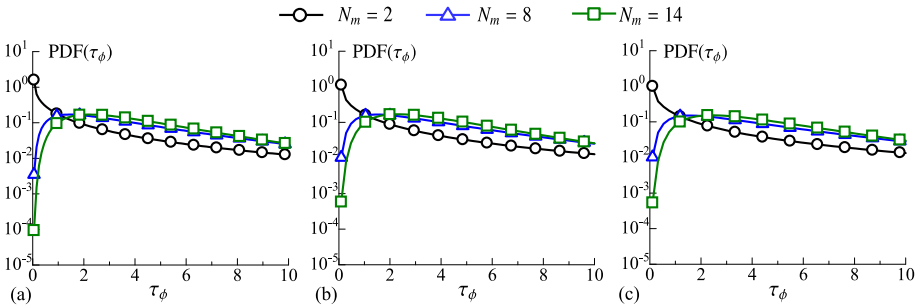

FIG. 13. The same plots as in Fig. 12 but for the MVM with $r_m = 70\eta$ on the jet centerline in (a) Run A (b) Run B, and (c) Run C.

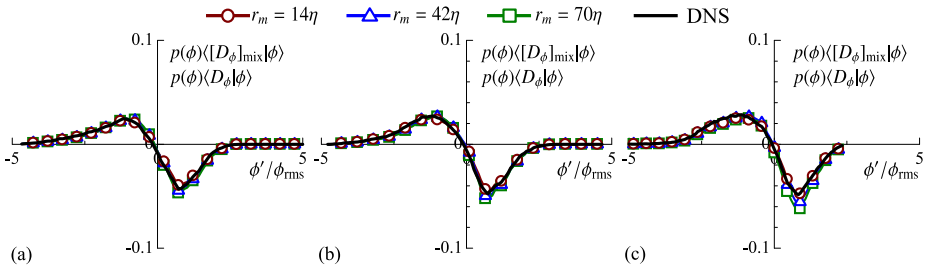

FIG. 14. Molecular diffusion density on the centerline from the DNS, $p(\phi)\langle D_\phi|\phi\rangle$, and the MVM, $p(\phi)\langle[D_\phi]_{\rm mix}|\phi\rangle$, with N_m = 14 in (a) Run A, (b) Run B, and (c) Run C. In each case, the plots are shown for $r_m = 14\eta$, $r_m = 42\eta$, and $r_m = 70\eta$.

density is compared between D_ϕ and $[D_\phi]_{\rm mix}$ in Fig. 16(b). The results of the MVM overlap with the DNS data, and the MVM well predicts the mean effects of the molecular diffusion even in the intermittent region.

Figure 17 visualizes passive scalar ϕ on an x-y plane at $t = 6$, at which the jet has not reached the self-similar regime (also see Fig. 4). The flow structure is very different between the transitional region (Fig. 17) and the self-similar region (Fig. 2). Passive scalar ϕ sharply changes across the edge of the shear layer in Fig. 17. Figure 18 shows the results of *a priori* test at $t = 6$ away from the centerline ($y = b_\phi \approx 0.5$). The correlation at $t = 6$ is very similar to the one in the self-similar region. A qualitative feature of the mean effects of the molecular diffusion is also captured by the MVM as found from the relation between $p(\phi)\langle[D_\phi]_{\rm mix}|\phi\rangle$ and ϕ' in Fig. 18. However, we can see a distinct difference between the DNS and MVM values in Fig. 18 although this difference becomes smaller as the size of the mixing volume, r_m, decreases.

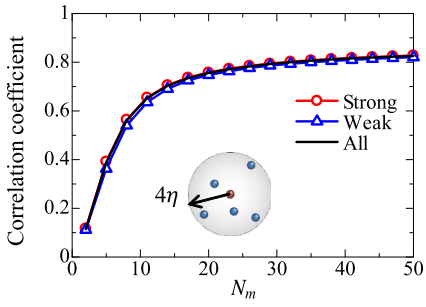

FIG. 15. Effects of fluid expansion and compression on the performance of the MVM. Correlation coefficients are computed for the molecular diffusion term between the DNS and MVM values (D_ϕ and $[D_\phi]_{\rm mix}$) for the mixing volumes with $r_m = 4\eta$ on the jet centerline of Run C. The results are separately presented for the mixing volume with $\langle\Theta|V_m^n\rangle > 0.5$ (strong case) and $\langle\Theta|V_m^n\rangle < 0.1$ (weak case). The correlation obtained from all mixing volumes is also shown for comparison.

We consider the performance of the MVM for the thermal conduction term written in the form of Eq. (17). Figure 7 has shown that the amplification process of the scalar gradient is statistically similar for the temperature and passive scalar. Therefore, we expect that the mixing time scales for temperature and scalar are also related to each other. The average within the mixing volume used in the MVM is related to the low-pass filtering. The mixing time scale in the mixing volume represents the time scale of the actual mixing process that occurs in the scale below the size of the volume.

Figure 19 shows the joint PDF of τ_ϕ and τ_T with N_m = 14 in Run D. A large probability can be seen around $\tau_\phi = \tau_T$, and τ_ϕ is positively correlated with τ_T. As the size of the mixing volume, r_m, increases, a peak location of the joint PDF is shifted toward large τ_ϕ and τ_T, indicating that τ_ϕ and τ_T tend to be larger and the molecular diffusion and

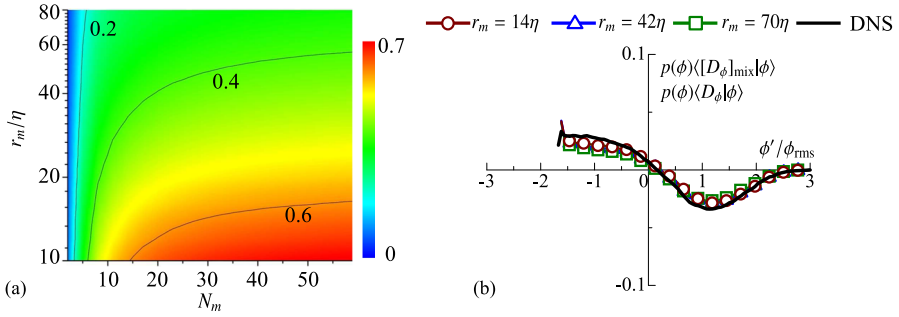

FIG. 16. Test of the MVM at $y = b_\phi$ in the self-similar region ($t = 22$ of Run B): (a) correlation coefficient between DNS and MVM values (D_ϕ and $[D_\phi]_{\rm mix}$) and (b) molecular diffusion density from DNS, $p(\phi)\langle D_\phi|\phi\rangle$, and MVM, $p(\phi)\langle[D_\phi]_{\rm mix}|\phi\rangle$, with $N_m = 14$. In (b), the plots are shown for $r_m = 14\eta$, $r_m = 42\eta$, and $r_m = 70\eta$.

thermal conduction become slower. This is consistent with a physical picture of the diffusion since these diffusive effects are dominated by small scales, and it takes longer time for these effects to affect a scalar distribution in larger scales. In the applications of the MVM to the Lagrangian simulations, it is required to model the scalar dissipation rate averaged in the mixing volume. Several models have been proposed for the passive scalar dissipation rate in the context of LES.[54] However, modeling the dissipation rate of temperature fluctuation is more challenging because of complexity in the equation for the temperature gradient. A positive correlation between τ_ϕ and τ_T indicates that a simple approach with approximation $\tau_T \approx \tau_\phi$ can be useful in the implementation of the MVM for the thermal conduction term.

The performance of the MVM for the thermal conduction is tested in a similar way to the molecular diffusion. The correlation coefficients of D_T between the DNS and MVM are shown in Fig. 20(a), while the joint PDFs for $r_m = 14\eta$ are shown in Fig. 21(a). The magnitude of the correlation and dependence of the correlation and joint PDF on N_m and r_m are very similar to those obtained for the molecular diffusion in Figs. 9–11. These results confirm that the MVM can provide a good estimation of molecular and thermal diffusions in compressible flows.

Since a simple model for the passive scalar dissipation rate based on the equilibrium assumption of scalar variance may not be applied to the dissipation rate of temperature fluctuations, computing mixing time scale τ_T is not easy in the application of the MVM. The joint PDF in Fig. 19 suggests that a simple estimation of τ_T is given by $\tau_T \approx \tau_\phi$. We consider the MVM for D_T with the mixing time scale given by $\tau_T = \tau_\phi$. The correlation coefficients and joint PDFs between the DNS and MVM values of D_T are computed with Run D, where the MVM with τ_T computed from the definition, Eq. (18), is compared with the one based on the assumption $\tau_T = \tau_\phi$ [Figs. 20(b) and 21(b)]. The MVM with $\tau_T = \tau_\phi$ also yields the thermal conduction term well correlated to the DNS value. The magnitude of the correlation in Fig. 20(a) is similar to the one obtained with $\tau_T = \tau_\phi$ in Fig. 20(b). Thus, the MVM with the assumption of $\tau_T = \tau_\phi$ still gives a good approximation of the thermal conduction term in Figs. 20(b) and 21(b) although the correlation is slightly weakened by the assumption of $\tau_T = \tau_\phi$ as found from comparison between Figs. 20(a) and 20(b). Figure 22 shows the conditional average $p(T)\langle[D_T]_{\rm mix}|T\rangle$ against $T' = T - \langle T\rangle$ computed with (a) τ_T given by Eq. (18) and (b) $\tau_T = \tau_\phi$. The MVM with Eq. (18) shows a good agreement with the DNS under various conditions, and the mean contribution of the diffusive effect is well captured by the MVM. However, the MVM with $\tau_T = \tau_\phi$ for $r_m = 14\eta$ [Fig. 22(b)] cannot capture the maximum and minimum values of the DNS results unlike the ones for $r_m = 42\eta$ and $r_m = 70\eta$.

Figures 20 and 22 indicate that usage of $\tau_T = \tau_\phi$ hardly affects the MVM for the thermal conduction with a large size of the mixing volume (large r_m). This is explained by the PDFs of τ_ϕ and τ_T shown in Fig. 23. The PDFs of τ_ϕ and τ_T are very different for small mixing volumes in Fig. 23(a) while they collapsed on a single curve for large mixing volumes in Fig. 23(b). It should be noted that the mixing time scale used in the MVM is related to the mixing in a scale below a size of the mixing volume. The PDF for small scales in Fig. 23(a) suggests that there are local differences in molecular and thermal diffusions in small scales, which is also related to spatial intermittency of the scalar dissipation rate.[5] Differences in governing equations and initial/boundary conditions between ϕ and T lead to different spatial distributions of intermittent small-scale structures with large dissipation rates of scalar and temperature fluctuations, which causes the difference in the PDFs of τ_ϕ and τ_T. However, the PDF in Fig. 23(b) indicates that the diffusive effects averaged over a large volume are similar for both molecular diffusion and thermal conduction because the large mixing volume can contain a large number of these structures with large scalar and temperature dissipation rates. Thus, the assumption of $\tau_T = \tau_\phi$ is crucial when we are

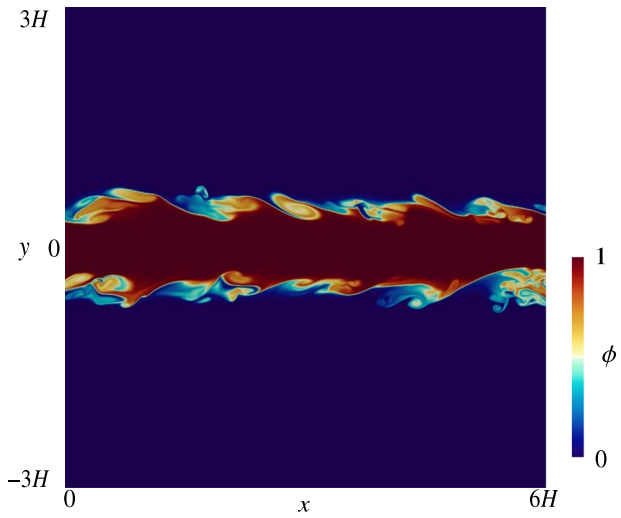

FIG. 17. Visualization of the passive scalar field at $t = 6$ (Run B).

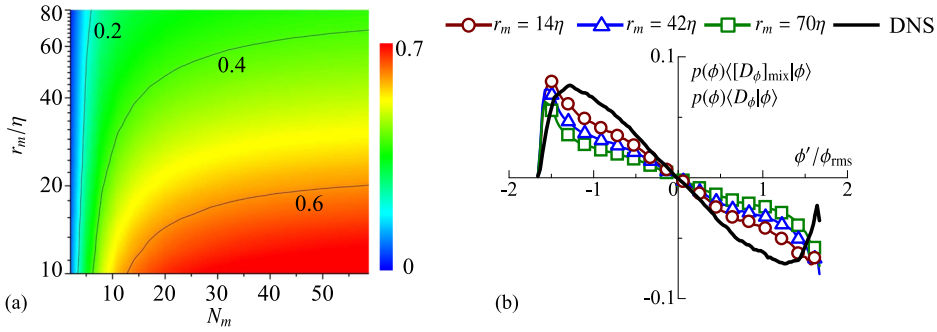

FIG. 18. Test of the MVM at $y = b_\phi$ in the transitional region ($t = 6$ of Run B): (a) correlation coefficient between DNS and MVM values (D_ϕ and $[D_\phi]_{\rm mix}$) and (b) molecular diffusion density from DNS, $p(\phi)\langle D_\phi|\phi\rangle$, and MVM, $p(\phi)\langle[D_\phi]_{\rm mix}|\phi\rangle$, with $N_m = 14$. In (b), the plots are shown for $r_m = 14\eta$, $r_m = 42\eta$, and $r_m = 70\eta$.

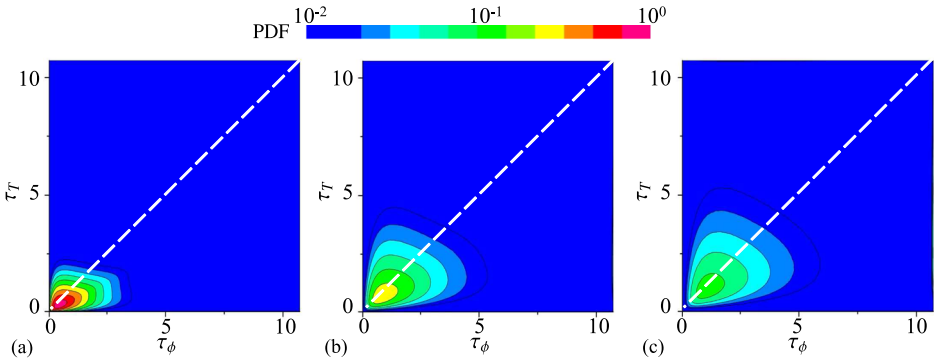

FIG. 19. Joint probability density functions of τ_ϕ and τ_T for $N_m = 14$ on the jet centerline in Run D with (a) $r_m = 14\eta$, (b) $r_m = 42\eta$, and (c) $r_m = 70\eta$. The broken line denotes $\tau_\phi = \tau_T$.

interested in modeling of the diffusive effects on temperature distributions in small scales. However, in typical simulations with the MVM, the size of the mixing volume is much larger than the dissipative scales.[26] This infers that $\tau_T = \tau_\phi$ can be a useful approximation for applying the MVM to the thermal conduction in compressible turbulence.

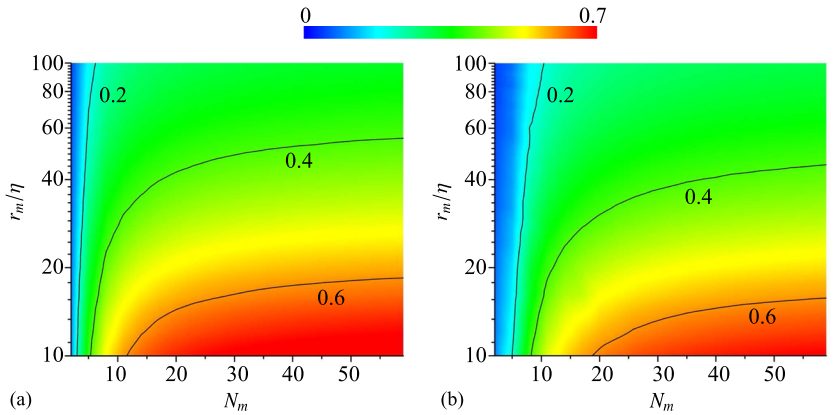

FIG. 20. Correlation coefficients between DNS and MVM values (D_T and $[D_T]_{\rm mix}$) for thermal conduction, where the MVM is computed with (a) τ_T in Eq. (18) and (b) assumption of $\tau_T = \tau_\phi$. The results are taken on the centerline of Run D.

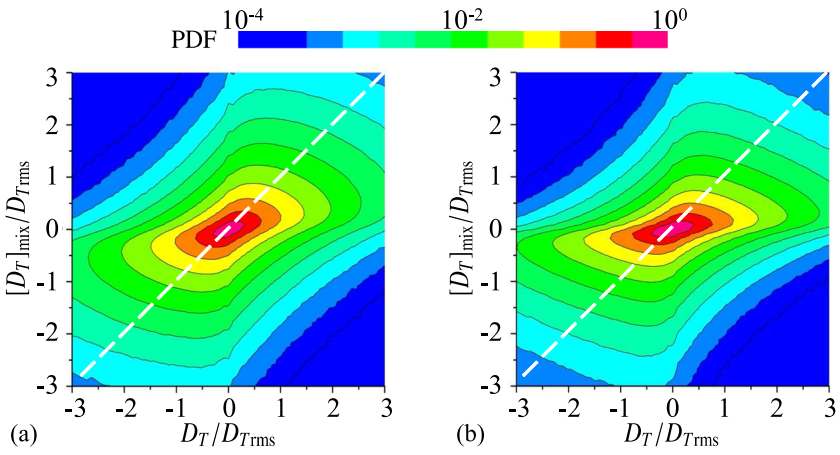

FIG. 21. Joint probability density functions of DNS and MVM values (D_T and $[D_T]_{\rm mix}$) of thermal conduction, where the MVM with $(N_m, r_m) = (14, 14\eta)$ is computed with (a) τ_T in Eq. (18) and (b) assumption of $\tau_T = \tau_\phi$. The results are taken on the centerline of Run D.

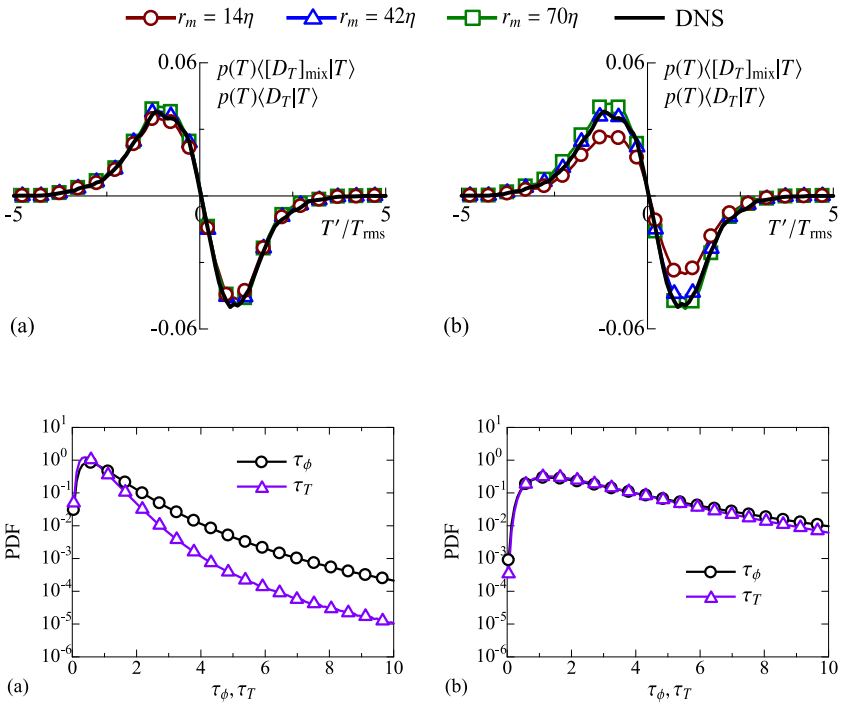

FIG. 22. Thermal conduction density obtained from DNS $p(T)\langle D_T|T\rangle$ and MVM $p(T)\langle[D_T]_{\rm mix}|T\rangle$ with $N_m = 14$, where the MVM with $(N_m,\ r_m) = (14,\ 14\eta)$ is computed with (a) τ_T in Eq. (18) and (b) assumption of $\tau_T = \tau_\phi$. The results are taken on the centerline of Run D.

FIG. 23. Probability density functions of mixing time scales τ_ϕ and τ_T on the jet centerline in Run D with $N_m = 14$ for (a) $r_m = 14\eta$ and (b) $r_m = 70\eta$.

VI. CONCLUDING REMARKS

We extend the mixing volume model (MVM) to compressible flows, where the diffusive effects arising from molecular diffusion and thermal conduction are of great interest in modeling issues in Lagrangian simulations of turbulent reactive flows. The MVM is based on the interaction among multiple particles within a mixing volume with a finite size, where the rate of the mixing is controlled by the mixing time scale within the volume (τ_ϕ for passive scalar ϕ and τ_T for temperature).

The MVM is tested using the DNS database of compressible turbulent planar jets with the jet Mach number ranging from 0.6 to 2.6. We show that the MVM well predicts the molecular diffusion term for passive scalar governed by the convection-diffusion equation in the fully developed compressible jets. In the transitional region of the jet, where the scalar field exhibits a sharp jump at the edge of the shear layer, a smaller mixing volume is required for an accurate prediction of mean effects of molecular diffusion. As expected from the study of the MVM for incompressible flows,[29] the prediction by the MVM is improved as the number of the mixing particles increases for a fixed volume size and as the size of the volume decreases for a fixed number of the mixing particles. A similar tendency is observed for the MVM formulated for thermal conduction. We show a strong similarity between the PDFs of the production of the dissipation rate of passive scalar and temperature fluctuations, where the production of both dissipation rates is dominated by the solenoidal part of strain that is coupled with scalar gradients. Therefore, the MVM for thermal conduction is also tested with the mixing time scale approximation $\tau_T = \tau_\phi$. The DNS results support $\tau_T \approx \tau_\phi$ for a wide range of scales of mixing volume. Therefore, the MVM with $\tau_T = \tau_\phi$ also well predicts the thermal conduction term. We find that the performance of the MVM with $\tau_T = \tau_\phi$ is degraded for very small mixing volumes. This is explained by the difference between the PDFs of τ_T and τ_ϕ for small scales, which is caused by different distributions of intermittent, small-scale structures of large dissipation rates. The PDFs of τ_T and τ_ϕ are almost identical for a large mixing volume, which can contain a large number of small-scale structures. Because of difficulty in modeling τ_T in the application of the MVM, the assumption of $\tau_T = \tau_\phi$ can be useful in the implementation of the MVM in Lagrangian simulations combined with the LES.

ACKNOWLEDGMENTS

The numerical simulations presented in this manuscript were carried out on the high-performance computing system in Nagoya University and the high-performance computing system (NEC SX-ACE) in the Japan Agency for Marine-Earth Science and Technology. This work was partially supported by "Collaborative Research Project on Computer Science with High-Performance Computing in Nagoya University" and by MEXT KAKENHI Grant No. 16K18013.

[1]Z. Warhaft, "Passive scalars in turbulent flows," Annu. Rev. Fluid Mech. **32**, 203 (2000).
[2]K. R. Smith, K. Dutta, C. Chengappa, P. Gusain, O. Masera, V. Berrueta, R. Edwards, R. Bailis, and K. N. Shields, "Monitoring and evaluation of improved biomass cook stove programs for indoor air quality and stove performance: Conclusions from the household energy and health project," Energy Sustainable Dev. **11**, 5 (2007).
[3]N. K. Togun and S. Baysec, "Prediction of torque and specific fuel consumption of a gasoline engine by using artificial neural networks," Appl. Energy **87**, 349 (2010).
[4]K. K. Kuo, *Principle of Combustion*, 2nd ed. (Wiley-Interscience, Hoboken, New Jersey, 2005).
[5]Q. Ni, "Compressible turbulent mixing: Effects of compressibility," Phys. Rev. E **93**, 043116 (2016).
[6]O. Reynolds, "On the dynamical theory of incompressible viscous fluids and the determination of the criterion," Philos. Trans. R. Soc., A **186**, 123 (1895).

[7]H. G. Weller, G. Tabor, A. D. Gosman, and C. Fureby, "Application of a flame-wrinkling LES combustion model to a turbulent mixing layer," in *Twenty-Seventh Symposium (International) on Combustion* (The Combustion Institute, Pittsburgh, 1998), pp. 899–907.
[8]P. E. DesJardin and S. H. Frankel, "Large eddy simulation of a nonpremixed reacting jet: Application and assessment of subgrid-scale combustion models," Phys. Fluids **10**, 2298 (1998).
[9]D. Haworth, "Progress in probability density function methods for turbulent reacting flows," Prog. Energy Combust. Sci. **36**, 168 (2010).
[10]A. Klimenko, "On simulating scalar transport by mixing between Lagrangian particles," Phys. Fluids **19**, 031702 (2007).
[11]A. Y. Klimenko, "Lagrangian particles with mixing. II. Sparse-Lagrangian methods in application for turbulent reacting flows," Phys. Fluids **21**, 065102 (2009).
[12]M. Cleary and A. Y. Klimenko, "A generalised multiple mapping conditioning approach for turbulent combustion," Flow, Turbul. Combust. **82**, 477 (2009).
[13]D. H. Rowinski and S. B. Pope, "An investigation of mixing in a three-stream turbulent jet," Phys. Fluids **25**, 105105 (2013).
[14]R. O. Fox, *Computational Models for Turbulent Reacting Flows* (Cambridge University Press, Cambridge, 2003).
[15]D. W. Meyer, "A new particle interaction mixing model for turbulent dispersion and turbulent reactive flows," Phys. Fluids **22**, 035103 (2010).
[16]R. L. Curl, "Dispersed phase mixing: I. Theory and effects in simple reactors," AIChE J. **9**, 175 (1963).
[17]C. Dopazo and E. E. O'Brien, "An approach to the autoignition of a turbulent mixture," Acta Astronaut. **1**, 1239 (1974).
[18]S. B. Pope, "An improved turbulent mixing model," Combust. Sci. Technol. **28**, 131 (1982).
[19]O. Soulard, V. Sabel'nikov, and M. Gorokhovski, "Stochastic scalar mixing models accounting for turbulent frequency multiscale fluctuations," Int. J. Heat Fluid Flow **25**, 875 (2004).
[20]S. Subramaniam and S. B. Pope, "A mixing model for turbulent reactive flows based on Euclidean minimum spanning trees," Combust. Flame **115**, 487 (1998).
[21]S. B. Pope, "A model for turbulent mixing based on shadow-position conditioning," Phys. Fluids **25**, 110803 (2013).
[22]A. Y. Klimenko and S. B. Pope, "The modeling of turbulent reactive flows based on multiple mapping conditioning," Phys. Fluids **15**, 1907 (2003).
[23]A. Sirivat and Z. Warhaft, "The effect of a passive cross-stream temperature gradient on the evolution of temperature variance and heat flux in grid turbulence," J. Fluid Mech. **128**, 323 (1983).
[24]M. Sheikhi, T. Drozda, P. Givi, F. Jaberi, and S. B. Pope, "Large eddy simulation of a turbulent nonpremixed piloted methane jet flame (Sandia flame D)," Proc. Combust. Inst. **30**, 549 (2005).
[25]S. James, J. Zhu, and M. Anand, "Large eddy simulations of turbulent flames using the filtered density function model," Proc. Combust. Inst. **31**, 1737 (2007).
[26]T. Watanabe, Y. Sakai, K. Nagata, Y. Ito, and T. Hayase, "LES–Lagrangian particle method for turbulent reactive flows based on the approximate deconvolution model and mixing model," J. Comput. Phys. **294**, 127 (2015).
[27]T. Watanabe and K. Nagata, "LES–Lagrangian-particles-simulation of turbulent reactive flows at high Sc number using approximate deconvolution model," AIChE J. **62**, 2912 (2016).
[28]S. Stolz and N. A. Adams, "An approximate deconvolution procedure for large-eddy simulation," Phys. Fluids **11**, 1699 (1999).
[29]T. Watanabe and K. Nagata, "Mixing model with multi-particle interactions for Lagrangian simulations of turbulent mixing," Phys. Fluids **28**, 085103 (2016).
[30]Z. Wang, J. Zhou, J. Fan, and K. Cen, "Direct numerical simulation of ozone injection technology for NO_x control in flue gas," Energy Fuels **20**, 2432 (2006).
[31]E. D. Gonzalez-Juez, A. R. Kerstein, R. Ranjan, and S. Menon, "Advances and challenges in modeling high-speed turbulent combustion in propulsion systems," Prog. Energy Combust. Sci. **60**, 26 (2017).
[32]A. Kempf, M. Klein, and J. Janicka, "Efficient generation of initial-and inflow-conditions for transient turbulent flows in arbitrary geometries," Flow, Turbul. Combust.: Appl. Sci. Res. **74**, 67 (2005).
[33]Z. Wang, Y. Lv, P. He, J. Zhou, and K. Cen, "Fully explicit implementation of direct numerical simulation for a transient near-field methane/air diffusion jet flame," Comput. Fluids **39**, 1381 (2010).
[34]Z. Wang, P. He, Y. Lv, J. Zhou, J. Fan, and K. Cen, "Direct numerical simulation of subsonic round turbulent jet," Flow, Turbul. Combust. **84**, 669 (2010).
[35]A. Abdelsamie, G. Fru, T. Oster, F. Dietzsch, G. Janiga, and D. Thévenin, "Towards direct numerical simulations of low-Mach number turbulent reacting and two-phase flows using immersed boundaries," Comput. Fluids **131**, 123 (2016).
[36]G. Lodato, P. Domingo, and L. Vervisch, "Three-dimensional boundary conditions for direct and large-eddy simulation of compressible viscous flows," J. Comput. Phys. **227**, 5105 (2008).
[37]C. A. Kennedy and M. H. Carpenter, "Several new numerical methods for compressible shear-layer simulations," Appl. Numer. Math. **14**, 397 (1994).
[38]C. A. Kennedy and A. Gruber, "Reduced aliasing formulations of the convective terms within the Navier–Stokes equations for a compressible fluid," J. Comput. Phys. **227**, 1676 (2008).
[39]T. Watanabe, Y. Sakai, K. Nagata, and O. Terashima, "Experimental study on the reaction rate of a second-order chemical reaction in a planar liquid jet," AIChE J. **60**, 3969 (2014).
[40]L. Bradbury, "The structure of a self-preserving turbulent plane jet," J. Fluid Mech. **23**, 31 (1965).
[41]E. Gutmark and I. Wygnanski, "The planar turbulent jet," J. Fluid Mech. **73**, 465 (1976).
[42]B. Ramaprian and M. Chandrasekhara, "LDA measurements in plane turbulent jets," J. Fluid Eng. **107**, 264 (1985).
[43]M. van Reeuwijk and M. Holzner, "The turbulence boundary of a temporal jet," J. Fluid Mech. **739**, 254 (2014).
[44]M. Klein, A. Sadiki, and J. Janicka, "Investigation of the influence of the Reynolds number on a plane jet using direct numerical simulation," Int. J. Heat Fluid Flow **24**, 785 (2003).
[45]C. B. da Silva and J. C. F. Pereira, "Invariants of the velocity-gradient, rate-of-strain, and rate-of-rotation tensors across the turbulent/nonturbulent interface in jets," Phys. Fluids **20**, 055101 (2008).
[46]M. Kozul, D. Chung, and J. P. Monty, "Direct numerical simulation of the incompressible temporally developing turbulent boundary layer," J. Fluid Mech. **796**, 437 (2016).
[47]T. Watanabe, Y. Sakai, K. Nagata, Y. Ito, and T. Hayase, "Enstrophy and passive scalar transport near the turbulent/non-turbulent interface in a turbulent planar jet flow," Phys. Fluids **26**, 105103 (2014).
[48]J. B. Freund, S. K. Lele, and P. Moin, "Compressibility effects in a turbulent annular mixing layer. Part 1. Turbulence and growth rate," J. Fluid Mech. **421**, 229 (2000).
[49]G. Brethouwer, J. C. R. Hunt, and F. Nieuwstadt, "Micro-structure and Lagrangian statistics of the scalar field with a mean gradient in isotropic turbulence," J. Fluid Mech. **474**, 193 (2003).
[50]G. Gulitski, M. Kholmyansky, W. Kinzelbach, B. Lüthi, A. Tsinober, and S. Yorish, "Velocity and temperature derivatives in high-Reynolds-number turbulent flows in the atmospheric surface layer. Part 3. Temperature and joint statistics of temperature and velocity derivatives," J. Fluid Mech. **589**, 103 (2007).
[51]T. Watanabe, Y. Sakai, K. Nagata, Y. Ito, and T. Hayase, "Reactive scalar field near the turbulent/non-turbulent interface in a planar jet with a second-order chemical reaction," Phys. Fluids **26**, 105111 (2014).
[52]T. Watanabe, T. Naito, Y. Sakai, K. Nagata, and Y. Ito, "Mixing and chemical reaction at high Schmidt number near turbulent/nonturbulent interface in planar liquid jet," Phys. Fluids **27**, 035114 (2015).
[53]M. Gampert, V. Narayanaswamy, P. Schaefer, and N. Peters, "Conditional statistics of the turbulent/non-turbulent interface in a jet flow," J. Fluid Mech. **731**, 615 (2013).
[54]A. W. Cook and J. J. Riley, "Subgrid-scale modeling for turbulent reacting flows," Combust. Flame **112**, 593 (1998).